Communications in Physics, Vol. 35, No. 3 (2025), pp. 215-224
DOI: https://doi.org/10.15625/0868-3166/22683

Structure and soft magnetic properties of nanocrystalline $Fe_{73.5}Nb_2Ta_1Si_{13.5}B_9Cu_1$ alloy ribbons

N. N. Dinh[1], **N. Q. Hoa**[1], **N. D. Thien**[1], **N. V. Dung**[2], **T. V. Thang**[1], **T. T. Ngoc Anh**[1], **D. T. Kim Anh**[1], **N. T. Nghia**[1], **B. T. Son**[3] **and V. V. Hiep**[1,†]

[1]*Faculty of Physics, VNU University of Science, 334 Nguyen Trai, Thanh Xuan, Hanoi, Vietnam*

[2]*Faculty of Engineering Physics, Hanoi University of Science and Technology, 1 Dai Co Viet, Hai Ba Trung, Hanoi, Vietnam*

[3]*Institute of Physics, Vietnam Academy of Science and Technology, 10 Dao Tan, Hanoi, Vietnam*

E-mail: †vuonghiepcms@gmail.com

Received 10 April 2025; *Accepted for publication 9 July 2025*; *Published 19 September 2025*

Abstract. *The crystal structure and soft magnetic properties of thermomagnetic annealed $Fe_{73.5}Nb_2Ta_1Si_{13.5}B_9Cu_1$ alloy ribbons prepared by rapid cooling were investigated. X-ray diffraction results showed that the as-cast alloy strips had a completely amorphous structure, while the annealed samples formed α-Fe (Si) nanocrystals with sizes ranging from 8 to 11 nm. Differential scanning calorimetry analysis of the as-cast samples indicated an exothermic crystallization peak at 515˚C of the first crystallization stage corresponding to the formation of the α-Fe (Si) crystalline phase. The as-cast ribbon samples were annealed at 500˚C for 30, 40, and 50 minutes and in a saturation magnetic field of 10 Oe. The crystallinity of the alloy ribbons thermomagnetically annealed at 500˚C for 30 min was determined by DSC analysis to be 42%. The optimum annealing time at 500˚C in a saturated magnetic field for the amorphous alloy ribbons to achieve the best magnetic properties was 40 minutes. Under that condition, the α- Fe (Si) phase crystallized completely, and the material exhibited excellent soft magnetic properties, with a saturation induction of B_s = 1.45 T, coercivity H_c = 0.015 Oe, and maximum permeability μ_{max} = 551,500.*

Keywords: thermomagnetic annealing; amorphous ribbon; α-Fe(Si); crystallization; soft magnetic.

Classification numbers: 75.50.Kj; 75.75.-c.

1. Introduction

In 1988, Yoshizawa [1] studied FeSiNbCu amorphous alloy ribbons and found that they exhibited excellent soft magnetic properties due to the crystallization of α-Fe nanoparticles on the amorphous matrix after appropriate annealing. To this day, this type of amorphous and nanocrystalline alloy ribbon (Finemet) continues to attract strong interest from scientists around

the world [2–5]. Finemet has high permeability ($\mu \sim 10^5$), low coercive force ($H_c \sim 0.5\ A/m$), high saturation magnetization ($M_s \sim 1.2\ T$), almost zero saturation magnetostriction ($\lambda_s \sim 10^{-6}$), and low core loss, making it widely used in electronic devices, sensors, and the electrical industry [6,7]. In recent times, research is still being conducted on improving technology and changing the composition to enhance the magnetic qualities of this material. Gheiratmand et al. [8] analyzed the role of element addition or substitution in increasing the glass-forming ability of Finemet and improving its soft magnetic properties. In the alloy ribbons, the element Cu plays a role in nucleating crystallization during annealing, while the element Nb, with its high melting point, functions to control the growth of crystal grains. The lattice constants of these phases increase with increasing tantalum content; however, the size of the crystal grains remains almost unchanged. It was shown in [9] that the first crystallization process corresponding to the formation of the α-Fe (Si) magnetic phase in the sample with tantalum content $x = 1$ occurred in a wider temperature range (~147˚C) compared to the other samples $x = 2, 3$. This allows the selection of the sample annealing temperature in a wider temperature range and is convenient for the manufacturing technology.

In addition, according to the paper [9], the lattice parameters of all crystal phases in Ta-substituted Finemet increase with increasing Ta content ($x = 1$, 2, 3), and the largest increase in lattice parameter values occurs for the Fe_3B boride crystal phase (the phase that deteriorates the magnetic properties).

Since the authors of [9] have not yet studied the effects of Ta substitution and the effects of magnetic annealing on the magnetic properties of Finemet, in this study we present a study on the crystal structure, crystallization process, and soft magnetic properties of $Fe_{73.5}Nb_2Ta_1Si_{13.5}B_9Cu_1$ alloy ribbons prepared by rapid cooling and subsequent annealing in a saturated magnetic field. Finemet composition with the smallest Ta content, x=1, substituted for Nb was chosen for study to minimize the influence of structural changes on the relevant properties, especially mechanical properties. We will show that magnetic annealing at appropriate temperature and time is a good technology to enhance the soft magnetic qualities of Finemet.

2. Experiment

The raw materials used for the production of alloy ribbons are the elements Fe, Nb, Si, Ta, B, and Cu in granular form of 2 to 4 mm in size with a purity of 3N to 4N, weighed according to their nominal composition. The alloy ribbons are fabricated using a rapid quenching technology on a single copper wheel, with each sample weighing 50 g. The fabrication conditions are similar to those of Finemet in our previous publication [2]. The alloy is melted at 1350˚C, and Ar gas at 1.15 atm is used to spray the molten alloy onto the surface of the rotating copper drum at a speed of 30 m/s. The resulting alloy ribbons have a width of 15 mm, a thickness of 20 μm, and a length greater than 1 m. The alloy ribbon samples were annealed in a saturated magnetic field (H = 10 Oe) and under a protective Ar atmosphere at 500˚C for 30, 40, and 50 minutes.

The structure of the alloy ribbons before and after annealing was examined using an X-ray diffractometer (Empyrean). Thermal phase transitions and the crystallization fraction of the alloy ribbons were analyzed using differential scanning calorimetry, DSC (Thermoplus EV02). A laboratory measurement system has been established to determine the hysteresis loop of ultra-soft magnetic materials such as Finemet. The system diagram is shown in Fig. 1 based on the method given in references [10, 11]. A sample consists of a toroidal core designed with a small

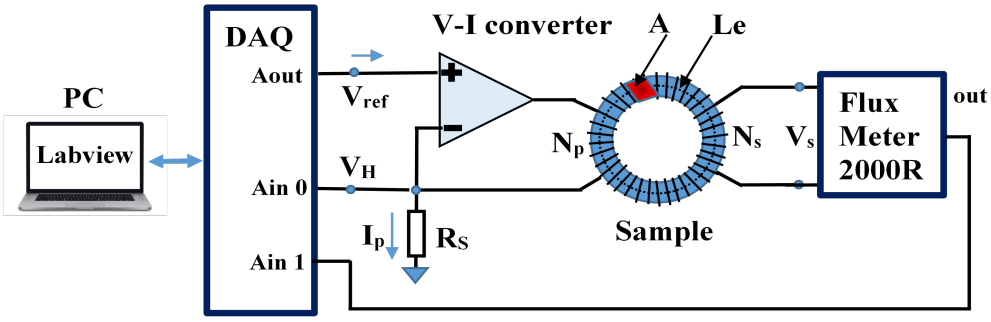

Fig. 1. Laboratory BH hysteresis measurement set up.

thickness-to-radius ratio to ensure uniform magnetic induction within the core, resulting in a demagnetization factor approximately equal to zero. The core is wound with two coils of equal turns, designated as the primary and secondary coils, respectively. A voltage-to-current converter, implemented using an OPA549 operational amplifier (Texas Instruments, USA), regulates the excitation current in the primary coil. This current is driven by an arbitrary waveform generated by the NI USB-6366 data acquisition module (National Instruments, USA). The excitation current is determined by measuring the voltage drop across a 1 $\Omega \pm 1\%$ shunt resistor connected in series with the primary coil. The magnetic flux density is measured directly using an FMI-2000R fluxmeter (Denshijiki Industry Co., Ltd., Japan). The measurement procedures are implemented as follows: (1) the ring core is demagnetized by applying an exciting current sufficiently large to create a magnetic field strength greater than ten times the H_c of the core. The exciting current is then slowly and smoothly reduced to zero to demagnetize the core. The used frequency is the same as the test frequency; (2) simultaneously with the generation of the arbitrary current waveform, data is acquired and processed using LabVIEW software to derive symmetric major and minor B-H loops; (3) from these hysteresis curves, fundamental parameters of soft magnetic materials, including initial magnetization curve, μ, B_s, and H_c, are calculated with an accuracy of 5%.

3. Results and discussion

Figure 2 shows the X-ray diffraction pattern of the $Fe_{73.5}Nb_2Ta_1Si_{13.5}B_9Cu_1$ sample immediately after fabrication (as-cast sample). The broad and faint peaks near $2\theta \approx 45^\circ$ and $2\theta \approx 65^\circ$ in the X-ray diffraction pattern are evidence of the amorphous structure of the as-cast sample. Those diffraction peaks after annealing of the as-cast sample become sharper, corresponding to bcc α-Fe (Si) nanocrystals: (110) 44.99°; (200) 65.70° (see also [9]).

DSC analysis of the as-cast $Fe_{73.5}Nb_2Ta_1Si_{13.5}B_9Cu_1$ alloy ribbon was carried out from room temperature to 650°C at a heating rate of 5°C/min. In Fig. 3, the first exothermic crystallization peak appears at T_1=515°C. The starting (T_{1S}=501°C) and ending (T_{1E}=550°C) temperatures of the first crystallization are determined by drawing the steepest tangents to the rising and falling edges of the first exothermic crystallization peak and extrapolating the intersection points to the baseline. The exothermic peak at T_1 = 515°C corresponds to the formation of the α-Fe(Si) crystalline phase in the amorphous ribbons during the first crystallization stage.

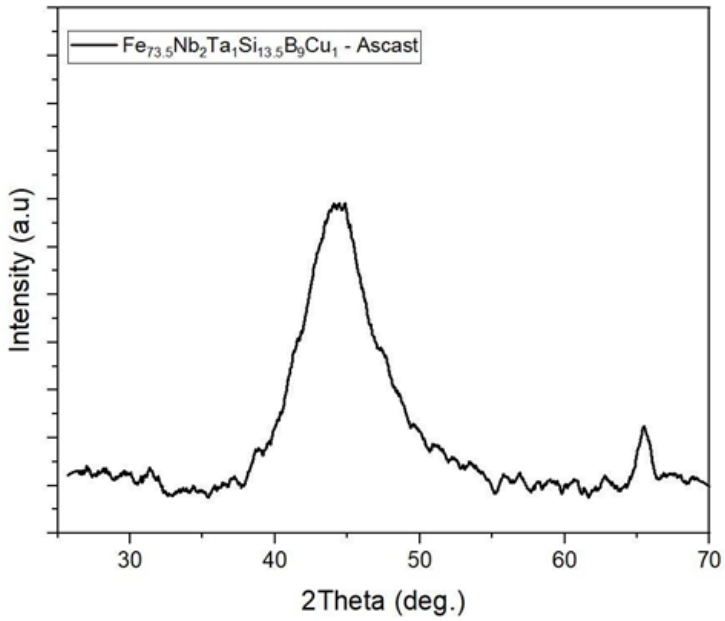

Fig. 2. X-ray diffraction patterns of as-cast $Fe_{73.5}Nb_2Ta_1Si_{13.5}B_9Cu_1$ ribbon.

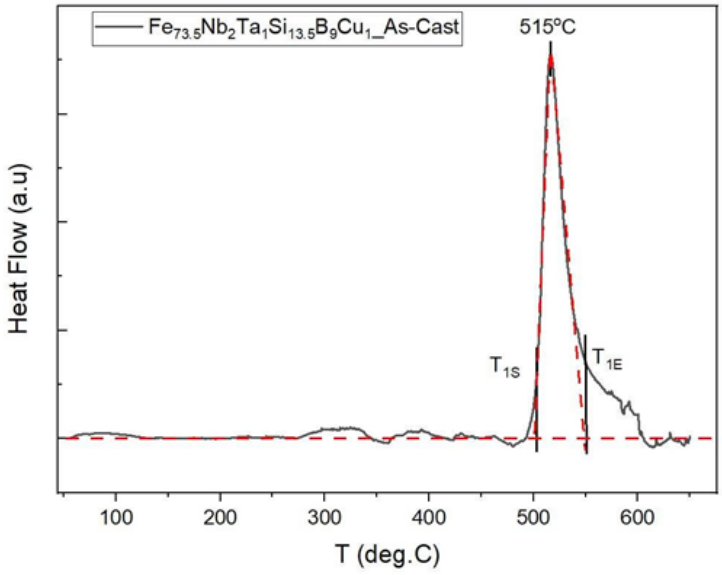

Fig. 3. DSC curves of as-cast $Fe_{73.5}Nb_2Ta_1Si_{13.5}B_9Cu_1$ ribbon with a heating rate of 5˚C/min.

This result is consistent with the studies on the primary crystallization stage of the tantalum-doped Finemet [9] and the Finemet series $Fe_{73.5}Si_{13.5}B_9Nb_3Ag_1$ [12] and $Fe_{87-x}Si_xB_9Nb_3Cu_1$ ($x =$

5, 7, 9, 13.5) [13]. Based on the DSC diagram for the as-cast sample, we determined the annealing conditions for the alloy ribbons as follows: annealing at T_a=500˚C for t=30, 40, and 50 minutes in a magnetic field of 10 Oe (thermomagnetic annealing - TMA) and in an argon protective gas environment.

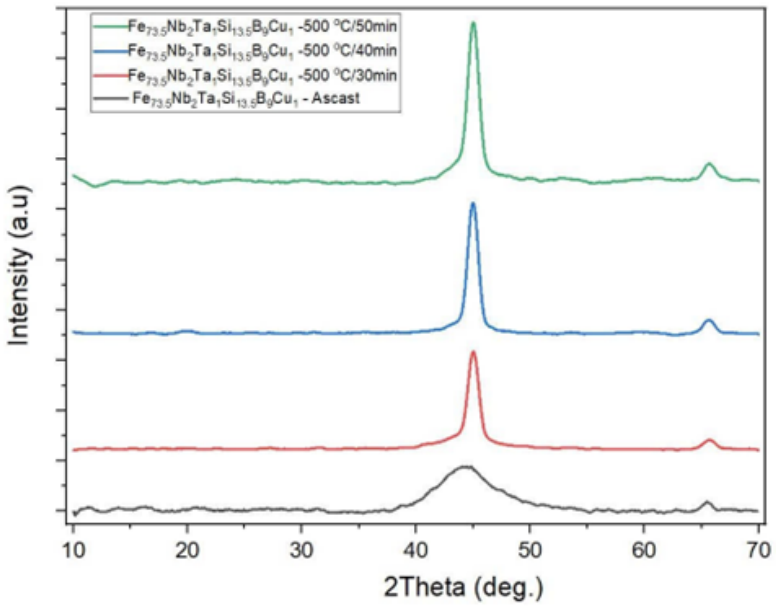

Fig. 4. X-ray diffraction patterns of the as-cast and thermomagnetic annealing $Fe_{73.5}Nb_2Ta_1Si_{13.5}B_9Cu_1$ ribbons.

Figure 4 shows the X-ray diffraction patterns of $Fe_{73.5}Nb_2Ta_1Si_{13.5}B_9Cu_1$ ribbons annealed in a magnetic field for different time periods. Two sharp peaks were observed at $2\theta = 45^\circ$ and 65°, indicating that the desired ferromagnetic α-Fe (Si) crystalline phase had formed in the ribbon. The average size D of the formed crystalline particles can be estimated using Fig. 4 and the Scherrer formula [14]

$$D = \frac{0.9\lambda}{\beta cos(\theta_\beta)}, \tag{1}$$

where $\lambda = 1.54056$Å is the X-ray wavelength, β in radians is the width of the spectral peak at half maximum intensity (FWHM) after subtracting the instrument broadening, and θ_β is the diffraction peak angle position. The average size of the α-Fe (Si) crystalline particles of the samples annealed at 500˚C for 30, 40, and 50 min is 8, 9, and 11 nm, respectively.

Figure 5 shows the DSC patterns of the as-cast sample and the samples annealed at 500˚C for 30 and 40 minutes in a magnetic field (denoted as 500˚C/30 min and 500˚C/40 min). The starting and ending temperatures of crystallization were determined by the tangent method, as shown in Figure 3. The starting temperature of the first crystallization of the 500˚C/30 min sample, T_{1S}=495˚C, is slightly lower than that of the as-cast sample. This is because annealing reduces internal stresses and increases the mobility of atoms in the amorphous structure. On the other

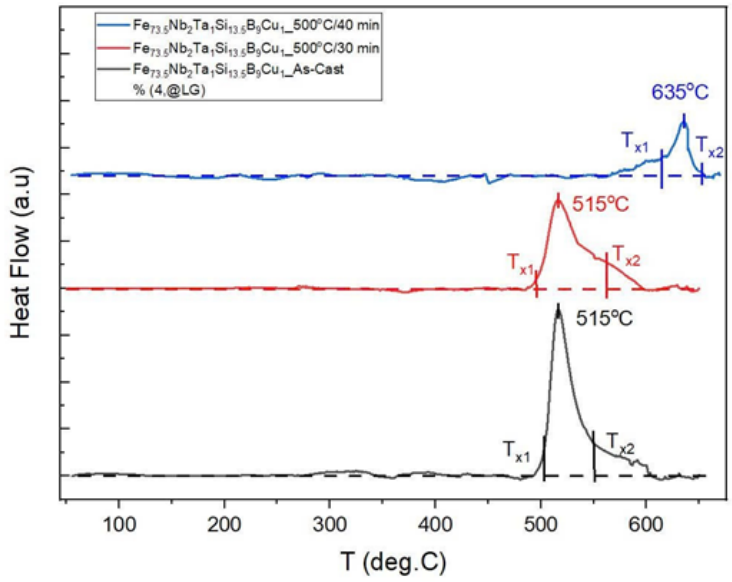

Fig. 5. DSC diagrams of $Fe_{73.5}Nb_2Ta_1Si_{13.5}B_9Cu_1$ as-cast and TMA for 30- and 40-minute samples.

hand, annealing also creates new crystallization centers. These factors make it easier for atoms to arrange into a crystalline structure at lower temperatures. On the DSC diagram of the 500˚C/40 min sample, only one crystallization peak was observed at T_2= 635˚C, and the starting and ending temperatures of the crystallization process corresponding to this peak were T_{2S}= 613˚C and T_{2E}= 654˚C. Based on the study of [9], it can be assumed that the T_2 crystallization peak corresponds to the formation of the tetragonal Fe_3B crystal phase, while the crystallization peak of the α-Fe(Si) crystal phase was not observed. This proves that annealing at 500˚C in a saturated magnetic field for 40 minutes is sufficient for the α-Fe(Si) phase to crystallize completely. The characteristic temperatures for the crystallization processes of the as-cast and the annealed samples are listed in Table 1 for comparison.

The fraction of bcc α-Fe (Si) crystalline phase formed in the strips annealed at 500˚C was calculated based on the observed DSC curves of the samples in Fig. 5 using the equation of Leu and Chin [15]:

$$\chi_f = \frac{\Delta H_a - \Delta H_t}{\Delta H_a}, \tag{2}$$

where ΔH_a is the crystallization enthalpy of the alloy ribbon with an amorphous structure, and ΔH_t is the enthalpy of the alloy ribbon after annealing for time t. Figure 5 also illustrates the comparison of the first crystallization process area (broadened peak area with the bottom dashed line) on the DSC diagram to calculate the crystallization fraction of the TMA sample for 30 minutes and the as-cast sample.

The calculation results based on Fig. 5 and the data of Table 1 show that the 30-min annealed sample has the α-Fe (Si) crystal phase volume ratio of 42% compared to the amorphous as-cast sample. In samples annealed at 500˚C in a saturated magnetic field for longer periods

Table 1. Sample's characteristic temperatures of the crystallization stage.

	$Fe_{73.5}Nb_2Ta_1Si_{13.5}B_9Cu_1$					
	T_{1S} (°C)	T_1 (°C)	T_{1E} (°C)	T_{2S} (°C)	T_2 (°C)	T_{2E} (°C)
As-cast	501	515	550			
500°C/30 min	495	515	563			
500°C/40 min				613	635	654

(40, 50 min) the α-Fe(Si) crystalline phase was completely crystallized. The 42% fraction of the α-Fe(Si) crystalline phase is a suitable value to achieve total magnetostrictive compensation of the amorphous and crystalline phases in the ribbon. According to Herzer [16], the saturation magnetostriction (λ_s) of the two-phase alloys is determined by the expression:

$$\lambda_s = V_{cr}\lambda_s^{cr} + (1 - V_{cr})\lambda_s^{amor}, \tag{3}$$

where V_{cr} and $(1 - V_{cr})$ are the volume fractions of the crystalline and the amorphous phases, correspondingly. λ_s^{cr} and λ_s^{amor} are the saturation magnetostriction of the crystalline and the amorphous phase, respectively. λ_s^{amor} for iron-based alloys is always negative and λ_s^{cr} is positive when V_{cr} is greater than 30%, then $\lambda_s \approx 5 \times 10^{-6}$ and the near-zero magnetostriction condition of the nanocrystalline sample is achieved [4].

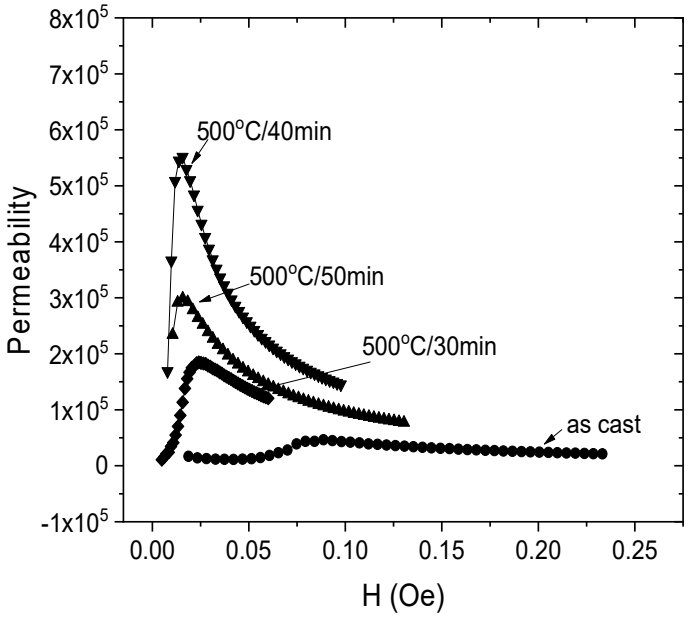

Fig. 6. Field dependence of the permeability of the as-cast and TMA samples.

Figure 6 presents the dependence of the permeability of $Fe_{73.5}Nb_2Ta_1Si_{13.5}B_9Cu_1$ alloy ribbon samples before and after TMA. It is found that the sample annealed at 500°C for 40 minutes has the largest maximum magnetic permeability (μ_{max} = 551,500).

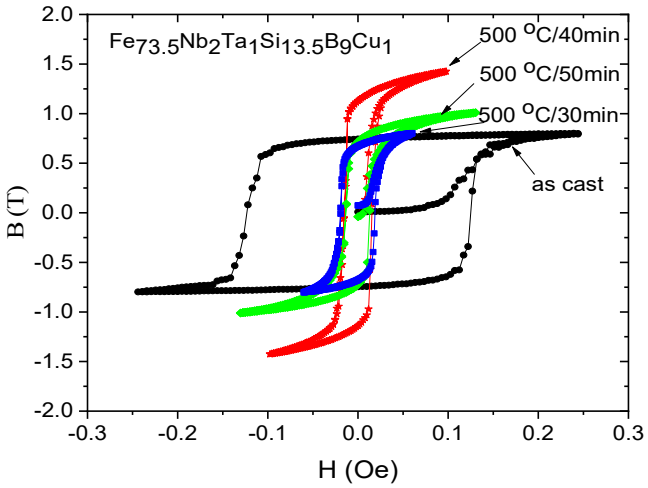

Fig. 7. Hysteresis loop B(H) of as-cast and TMA samples.

As shown in Fig. 7, the hysteresis loops of the TMA samples are much narrower, and their saturation magnetic inductions are much higher than those of the as-cast samples. Parameters such as maximum permeability, coercivity, and saturation magnetic induction of as-cast and TMA samples are listed in Table 2 in comparison with those of some other works. It is clear that the TMA samples exhibit significantly improved soft magnetic properties compared to the as-cast samples.

Table 2. Soft magnetic characteristics of some Finemet types.

Finemet Type		μ_{max}	H_c **(Oe)**	B_s **(T)**	**Reference**
$Fe_{73.5}Nb_2Ta_1Si_{13.5}B_9Cu_1$ [*)]	As-cast	43,200	0.120	0.79	Present work
	500°C/30 min	200,000	0.020	0.80	
	500°C/40 min	551,500	0.015	1.45	
	500°C/50 min	300,000	0.013	1.00	
$Fe_{73.5}Nb_3Cr_1Si_{13.5}B_9Cu_1$	540°C/30 min	50,000	0.069	1.08	[17]
Finemet FT-3M	(annealed)	70,000	0.031	1.23	[18]
$Fe_{73.5}Nb_3Si_{13.5}B_9Ag_1$	585°C/30 min	31,000	0.120	0.60	[12]
$Co_{65.5}Fe_{3.5}Cr_3B_{10}Si_{18}$	(annealed)	450,000	0.159	0.42	[19]
$Fe_{78}Nb_3Si_9B_9Cu_1$	520°C	1,512	0.140	1.51	[13]

[*)] Annealing in magnetic field $H = 10$ Oersted.

Notably, annealing at 500˚C for 40 min at a field of 10 Oe results in a saturation induction $B_s = 1.45$ T, coercivity $H_c = 0.015$ Oe, and maximum permeability $\mu_{max} = 551{,}500$. Before annealing Finemet in amorphous form, the amorphous magnetic grains are oriented randomly, with high losses. Annealing at 500˚C for 40 minutes in a magnetic field of 10 Oe along the length of the strip

may be the optimal condition for the most abundant, uniform α-Fe (Si) crystal grains with an average size of 8-11 nm in the amorphous matrix and their easy magnetization axis oriented in the magnetic field direction. This two-phase structure (α-Fe(Si) nanocrystals in a non-crystalline base) leads to strong magnetic interactions that balance out and significantly lower the effective magnetic anisotropy (which includes both magnetocrystalline anisotropy and magnetic field-induced anisotropy), decrease the coercivity (H_c), and make it easier for the magnetic moment to rotate at very low magnetic fields, resulting in higher permeability (μ). The soft magnetic properties of the 500˚C/40 min annealed sample were superior to those of the $Fe_{72.5}Cr_1Si_{13.5}B_9Nb_3Cu_1$ [17], Hitachi's FT-3M [18], $Fe_{73.5}Nb_3$ $Si_{13.5}B_9Ag_1$ [12], and cobalt-based $Co_{67}Fe_3Cr_3B_{11.5}Si_{15.5}$ [19] systems. Recently, Kwon and his colleagues [13] also fabricated amorphous $Fe_{78}Nb_3Si_9B_9Cu_1$ alloy ribbons and annealed them at 520˚C in the magnetic field. After annealing, the ribbons had a fairly high magnetic induction of 1.51 T, but the permeability was low and the coercive force was higher than that of our sample (see Table 2).

The experimental results for $Fe_{73.5}Nb_2Ta_1Si_{13.5}B_9Cu_1$ nanocrystalline ribbons can be understood in the context of Herzer's random magnetic anisotropy theory [20]. According to Herzer's model, the effective magnetic anisotropy $<K>$ of a two-phase disordered alloy in the case of small grains D ($D<L_{exc}$, L_{exc} is the exchange length) is proportional to the sixth power of the grain size

$$\langle K\rangle = \frac{{K_1}^4}{A^3}D^6, \tag{4}$$

$$L_{exc} \approx \sqrt{\frac{A}{\langle K\rangle}}, \tag{5}$$

where K_1 is the magnetocrystalline anisotropy constant, and A is the exchange stiffness. Therefore, the coercivity is proportional to the sixth power of the grain size, $H_c \sim D^6$. Using the data for K_1 and A of α-Fe-20 at% Si, Herzer estimated $L_{exc} \approx 40$ nm for the iron-based Finemet [20]. The grain size in our case satisfies the condition $D<L_{exc}$, so the coercivity of the material is very small and the magnetic permeability ($\mu \sim 1/H_c$) is very large.

4. Conclusion

Amorphous $Fe_{73.5}Nb_2Ta_1Si_{13.5}B_9Cu_1$ alloy ribbons were prepared by rapid cooling and magnetic annealing at 500˚C in a 10 Oe magnetic field for 30, 40, and 50 min. X-ray diffraction analysis showed the formation of α-Fe(Si) nanocrystals with sizes ranging from 8 to 11 nm. The crystallinity of the 30-min TMA sample was 42%, as determined by DSC measurements. The $Fe_{73.5}Nb_2Ta_1Si_{13.5}B_9Cu_1$ alloy after thermomagnetic annealing for 40 min achieved excellent soft magnetic properties with saturation induction $B_s = 1.45$ T, coercivity $H_c = 0.015$ Oe, and maximum permeability mu_{max} = 551,500, which is related to the complete crystallization of the α-Fe(Si) phase in the sample. The soft magnetic properties of the obtained material were explained based on the Herzer phenomenological theory and compared with the results given by other authors. The thermomagnetic annealed $Fe_{73.5}Nb_2Ta_1Si_{13.5}B_9Cu_1$ nanocrystalline ribbons have potential for use as highly sensitive magnetic sensors as well as other soft magnetic material applications.

Acknowledgments

The authors would like to thank the Physics Development Program for the period 2021 - 2025 for funding this research under the project code ĐTĐL.CN 27/23. Sincere thanks to Prof. Bach Thanh Cong for reading the manuscript and contributing valuable comments.

Conflict of interest

The authors have no conflicts of interest to declare.

References

[1] Y. Yoshizawa, S. Oguwa and K. Yamaguchi, *New Fe based soft magnetic alloys composed of ultrafine grain structure*, J. Appl. Phys. **64** (1988) 6044.
[2] N. Chau, N.X. Chien, N.Q. Hoa, P.Q. Niem, N.H. Luong, N.D. Tho *et al.*, *Investigation of nanocomposite materials with ultrasoft and high performance hard magnetic properties*, J. Magn. Magn. Mater. **282** (2004) 174.
[3] X. B. Zhai, L. Zhu, H. Zheng, Y. D. Dai, J. K. Chen, Y. G. Wang *et al.*, *Optimization of crystallization, microstructure and soft magnetic properties of Fe-B-Cu alloys by rapid cyclic annealing*, J. Alloys Compd. **768** (2018) 591.
[4] K. Suzuki, *Recent advances in nanocrystalline soft magnetic materials: A critical review for way forward*, J. Magn. Magn. Mater. **592** (2024) 171677.
[5] D. Azuma, N. Ito and M. Ohta, *Recent progress in Fe-based amorphous and nanocrystalline soft magnetic materials*, J. Magn. Magn. Mater. **501** (2020) 166373.
[6] Z. Huo, G. Zhang, J. Han, J. Wang, S. Ma and H. Wang, *A review of the preparation, machining performance, and application of Fe-based amorphous alloys*, Processes **10** (2022) 1203.
[7] J. M. Silveyra, E. Ferrara, D. L. Huber and T. C. Monson, *Soft magnetic materials for a sustainable and electric world,* Science **362** (2018) 418.
[8] T. Gheiratmand and H. R. Madaah Hosseini, *Finemet nanocrystalline soft magnetic alloy: Investigation of glass forming ability, crystallization mechanism, production techniques, magnetic softness and the effect of replacing the main constituents by other elements*, J. Magn. Magn. Mater. **408** (2016) 177.
[9] A. Puszkarz, M.Wasiak, A. Rózanski, P. Sovak and M. Moneta, *Structural and magnetic properties of Finemet^{TM} doped with Ta*, J. Alloys Compd. **491** (2010) 495.
[10] F. Fiorillo, *Measurements of magnetic materials*, Metrologia **47** (2010) S114.
[11] S. Li, F. Bielsa, M. Stock, A. Kiss and H. Fang, *An investigation of magnetic hysteresis error in Kibble balances*, IEEE Trans. Instrum. Meas. **69** (2020) 5717.
[12] N. Chau, N. Q. Hoa and N. H. Luong, *The crystallization in Finemet with Cu substituted by Ag*, J. Magn. Magn. Mater. **290-291** (2005) 1547.
[13] S. Kwon, S. Kim and H. Yim, *Improvement of saturation magnetic flux density in Fe–Si–B–Nb–Cu nanocomposite alloys by magnetic field annealing*, Curr. Appl. Phys. **20** (2020) 37.
[14] A. Patterson, *The Scherrer Formula for X-Ray Particle Size Determination*, Phys. Rev. **56** (1939) 978.
[15] M. S. Leu and T. S. Chin, *Quantitative Crystallization and Nano-Grain Size Distribution Studies of a Fecunbsib Nanocrystalline Alloy*, MRS Symp. Proc. **577** (1999) 557.
[16] G. Herzer, *Modern soft magnets:Amorphous and nanocrystalline material*, Acta Mater. **61** (2013) 718.
[17] N. Chau, P. Q. Thanh, N. Q. Hoa and N. D. The, *The existence of giant magnetocaloric effect and laminar structure in $Fe_{73.5-x}Cr_xSi_{13.5}B_9Nb_3Cu_1$*, J. Magn. Magn. Mater. **304** (2006) 36.
[18] https://hilltech.com/pdf/hl-fm10-cFinemetIntro.pdf
[19] A. V. Nosenko, V. V. Kyrylchuk, M. P. Semen'ko, M. Nowicki, A. Marusenkov, T. M. Mika *et al. Soft magnetic cobalt based amorphous alloys with low saturation induction*, J. Magn. Magn. Mater. **515** (2020) 167.
[20] G. Herzer, *Grain Size Dependence of Coercivity and Permeability in Nanocrystalline Ferromagnets*, IEEE Trans. Magn. **26** (1990) 1397.